Uncertainty issues in the experimental assessment of degradation rate of power ratings in photovoltaic modules

Uncertainty issues in the experimental assessment of degradation rate of power ratings in photovoltaic modules

A. Carullo [a,*], A. Castellana [a], A. Vallan [a], A. Ciocia [b], F. Spertino [b]

[a] Politecnico di Torino, Dipartimento di Elettronica e Telecomunicazioni, Corso Duca degli Abruzzi, 24, 10129 Torino, Italy
[b] Politecnico di Torino, Dipartimento Energia, Italy

A B S T R A C T

A test procedure is described in this paper that is conceived to investigate the degradation mechanism of PhotoVoltaic (PV) modules subjected to different stress quantities. The procedure is based on the appli-cation of environmental and mechanical stress quantities to the modules under investigation and on the electrical and optical characterization of the same modules. The measurement technique implemented to estimate the maximum power at Standard Test Conditions (STC) of the PV modules is deeply investigated in order to estimate the 95% confidence interval of the estimated parameter. Preliminary results are also reported that refer to the application of the proposed test procedures to two sets of p-Si modules.

1. Introduction

Despite of the world-wide growing use of PV plants for electrical energy production [1], parameters that allow the degradation rate of PV modules to be estimated on long time periods are rarely available. For thin-film based PV technologies, this kind of information is not provided, while for Si-based technologies the manufacturers often state a warranty in terms of maximum power warranted during the first 10 years and 25 years of operation, that is 90% and 80% of the initial maximum power, respectively. Unfortunately, information related to the phenomena responsible for this degradation and their time behavior are not known, thus not allowing a reliable estimation of the pay-back time of a PV plant to be obtained. In the scientific literature, experimental results are described that refer to outdoor exposed PV plants [2–5], but these results are only provided for Si-based modules and are based on the comparison between initial and final measurements after many years of operation in a non-controlled environment, thus not allowing the degradation trend to be estimated. An attempt in estimating such a trend has been made through the arrangement of the outdoor experimental PV laboratory described in [6,7], that has been conceived to monitor ten plants based on different PV technologies. The obtained results over a three-year period, which refer to both Si-based and thin-film based PV modules, are described on a monthly basis in [8]. These results can be summarized as follow:

- silicon technologies show lower degradation than thin-film technologies;
- string ribbon Si modules are more subjected to degradation than m-Si and p-Si modules;
- PV modules mounted on 2-axis tracking systems show higher degradation than the same PV modules mounted in fixed position.

The last result is in agreement with the conclusions in [9–11], where higher thermal and mechanical stresses are indicated as responsible for a fast degradation rate.

In order to better understand the degradation mechanisms of outdoor exposed PV modules, a series of laboratory tests and characterization procedures are here proposed. The tests are intended for reproducing outdoor conditions and also obtaining a convenient acceleration factor, thus minimizing the test time. The characterization procedures are based on the estimation of the electrical parameters of the tested PV modules and the application of the electroluminescence (EL) technique, which allows micro-cracking and other defects that result in power-loss to be identified. With respect to the test procedures described in [12], which are mainly conceived to simulate a long-term degradation of PV modules, this paper focuses on tests designed to identify

the PV degradation rate related to specific stresses. Particular attention is paid towards the uncertainty estimation of the measured parameters and useful tips are provided for a good selection of the measuring instrumentation.

2. Test procedure

The proposed test procedure is based on the application of different stress factors to a set of PV modules of the same technology. Initially, the samples of each set (at least five units) are characterized in order to obtain their $I-V$ characteristics and EL images. Then, the sample 1 is preserved by any stress in order to act as the reference module, while the other modules are subjected to environmental and mechanical stresses. At the end of each test cycle, all the modules of each set will be again characterized and the performance degradation will be estimated and correlated to each stress factor.

2.1. Stress tests

Environmental stresses are applied to two of the PV modules under test. The sample 2 is exposed to a damp-heat test, that is conceived to accelerate the water absorption in the PV module and then decrease its electrical insulation. The test is performed inside a climatic chamber that is set to perform a 24-h cycle with relative humidity always higher than 90% and temperature in the range of (25–55 °C). The sample 4 is instead subjected to thermal cycles in the range of −20 °C to 70 °C with a temperature rate of about 1 °C/ min (6 cycles during a 24-h test). The selected temperature ranges have been chosen according to the experimental conditions of the outdoor monitored PV laboratory.

The other two samples of the set under test are subjected to mechanical stresses. Dynamic load is applied to the sample 3, which is mounted on the vibrating table of an electrodynamic shaker, which is driven in order to perform 5-h random vibration cycles in the frequency range of (5–150 Hz) and a root mean square acceleration of 5 m/s^2. The sample 5 is instead subjected to a static stress, which is conceived to simulate a medium snow load. Other details about the applied stresses can be found in [13].

2.2. Optical characterization

With the aim of detecting the defects in the PV modules subjected to the stress tests, the electroluminescence (EL) technique is used. This technique is based on the application of a forward bias to a shaded PV module, which in this condition acts as a light emitting diode with an emission spectra in the range of about (950–1350 nm). A sensitive camera equipped with silicon charge-coupled device (CCD) or indium gallium arsenide (InGaAs) photodiodes is able to detect the emitted photons, thus obtaining an image where defective areas appear darker than perfect areas. In order to achieve a high signal-to-noise ratio and hence a clear image, the EL characterization of the PV modules has been performed inside a darkroom. The obtained images allow different defects to be highlighted, such as:

- micro cracks, which are mainly due to mechanical or thermal stresses and that usually evolve into broken cells;
- broken cells, which are characterized by electrically isolated areas that limit the current in the whole string;
- impurities and chain pattern, which are due to a low-quality production process and that appear like less shine areas in EL images;
- Potential Induced Degradation (PID), which is due to leakage currents with respect to earth, that in turn depend on high voltage and weather conditions.

2.3. Electrical characterization

The electrical characterization of a PV module is intended to obtain the current-voltage ($I-V$) characteristic of the module, which has to be referred to the Standard Test conditions (STC: standard spectrum $G_{STC} = 1000\ W/m^2$ and cell temperature $T_{STC} = 25\ °C$). Among the available methods for the $I-V$ characterization, the variable-load technique has been implemented in this work. In order to refer the obtained results to the STC, two different approaches can be considered. The first approach is based on the PV module characterization performed at the standard conditions, which requires a solar simulator inside a climatic chamber to be used. In this case, the employed equipment is very expensive, above all for the solar simulator, whose performance in terms of spectral distribution, irradiance uniformity and stability has to match the requirements of the document [14]. The second approach requires the PV module to be characterized in outdoor conditions, hence under the solar radiation, obtaining the $I-V$ characteristic at the measured irradiance G_m and environmental temperature T_e. This solution, which has been adopted by the authors, is affordable and simple, but requires a correction algorithm to be implemented in order to translate the $I-V$ curve from the measured conditions to the STC. Once the $I-V$ characteristic at STC has been estimated, the maximum power $P_{M,STC}$ is obtained, which is the parameter used to assess the performance of the PV module. The comparison among the $P_{M,STC}$ values obtained after the stress cycles allows the degradation rate related to each stress factor to be estimated.

In this framework, it is very important to highlight the main contributions that affect the uncertainty of the parameter $P_{M,STC}$, thus making reliable the estimation of the degradation rate. With this aim, the whole measuring process is revised and useful tips are provided in order to minimize the overall uncertainty.

2.3.1. Experimental set-up

The system that has been arranged for the electrical characterization of the modules under test, which is based on a programmable electronic load connected to the PV module, is shown in the Fig. 1. The current I_m the module provides and the voltage V_m across the module are measured by means of two 6 and 1/2 digit multimeters DMM1 (Fluke model 8846A) and DMM2 (Agilent model 34401A), while the irradiance G_m is sensed through a secondary standard pyranometer, whose voltage output is measured by means of another 6 and 1/2 digit multimeter DMM3 (Agilent model 34401A). All the multimeters and the programmable load are connected through a standard IEEE-488 interface to a Personal Computer, where a program runs that drives the load and acquires voltage, current and irradiance measurements. The environmental temperature T_e is sensed through a thermometer based on a Pt-100 resistive thermal detector and the cell temperature T_m is estimated using the parameter *NOCT* (Nominal Operating Cell Temperature) of the module under test. The expanded uncertainties (coverage factor $k = 2$) of the measured quantities are summarized below:

- irradiance G_m, 1.3% of reading and maximum offset of 7 W/m^2;
- voltage V_m, 20 ppm of reading and maximum offset of 10 μV;
- current I_m, 0.1% of reading and maximum offset of 40 μA;
- cell temperature T_m, 2 °C.

2.3.2. Correction algorithm

The algorithm that has been implemented to translate the measured $I-V$ characteristics to the STC is based on the procedure 1 suggested in the document [15]. The current and voltage values I_{STC} and V_{STC} at STC are obtained from the measured current and voltage values I_m and V_m by means of the following expressions:

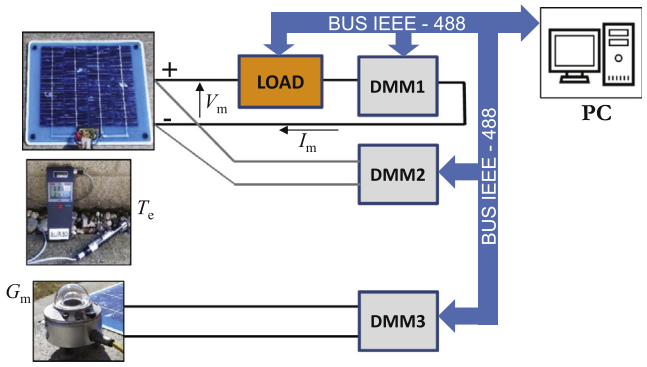

Fig. 1. Block scheme of the experimental set-up.

$$I_{STC} = I_m + I_{sc,m} \cdot \left(\frac{G_{STC}}{G_m} - 1\right) + \alpha \cdot (T_{STC} - T_m)$$
$$V_{STC} = V_m + \beta \cdot (T_{STC} - T_m) - R_S \cdot (I_{STC} - I_m) \quad (1)$$

where

- $I_{sc,m}$ is the short circuit current at measured conditions (A);
- α is the thermal coefficient of current (A/°C);
- β is the thermal coefficient of voltage (V/°C);
- R_S is the series resistance of the PV module (Ω).

The parameters $I_{sc,m}$ and R_S are obtained by extrapolating the measured values, as highlighted in the Fig. 2, where the square boxes represent the measured voltage and current values and the black line is the $I-V$ characteristic at STC. In the same figure, the red line close to the short circuit condition represents the extrapolated curve that allows the short circuit current $I_{sc,m}$ of the PV module to be obtained, while the red line close to the open-circuit voltage V_{oc}, m is the extrapolated curve whose slope is the reciprocal of the series resistance R_S.

Once the $I-V$ curve at STC has been obtained, the corresponding $P-V$ curve can be drawn and the parameter $P_{M,STC}$ is obtained as the maximum value, as shown in the Fig. 3.

3. Uncertainty estimation

The procedure described in the Section 2.3 can be summarized by means of the measurement model $f(.)$:

$$P_{M,STC} = f(G_m, T_m, I_m, V_m; G_{STC}, T_{STC}, \alpha, \beta) \quad (2)$$

This model highlights that the uncertainty of the parameter $P_{M,STC}$ depends on several contributions, which can be subdivided into four categories:

- measurement uncertainty of the quantities G_m, T_m, I_m and V_m; one should note that the last two quantities also affect the estimation of the parameters $I_{sc,m}$ and R_S that are obtained by extrapolating the measured curve;
- uncertainty in the knowledge of the PV module parameters α and β;
- model uncertainty, i.e. the uncertainty that is due to the non perfect description of the PV module behavior by means of the correction algorithm (1);
- repeatability contributions, which are mainly due to the noise superimposed to the measured signals.

However, since the results of the present work are based on the comparison of the parameter $P_{M,STC}$ of each PV module estimated after each stress cycle, the contributions related to the module parameters α and β and to the model uncertainty can be considered negligible. This assumption has been strengthen by choosing irradiance G_m in measurement conditions not lower than the 75% of G_{STC}.

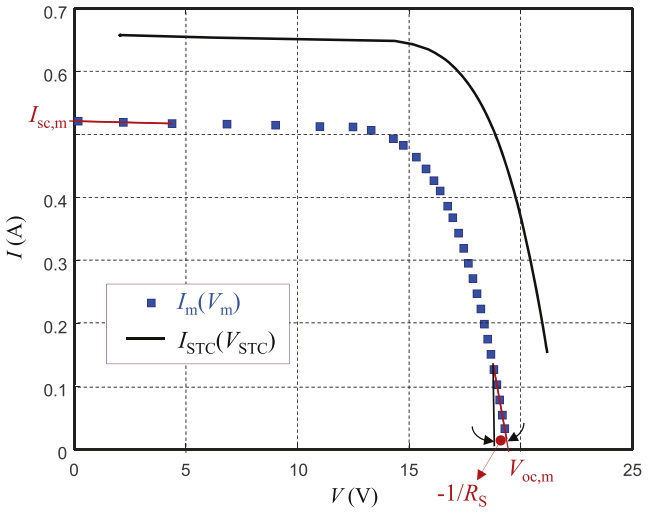

Fig. 2. Example of $I-V$ curves at measured conditions (square boxes) and at STC (black line).

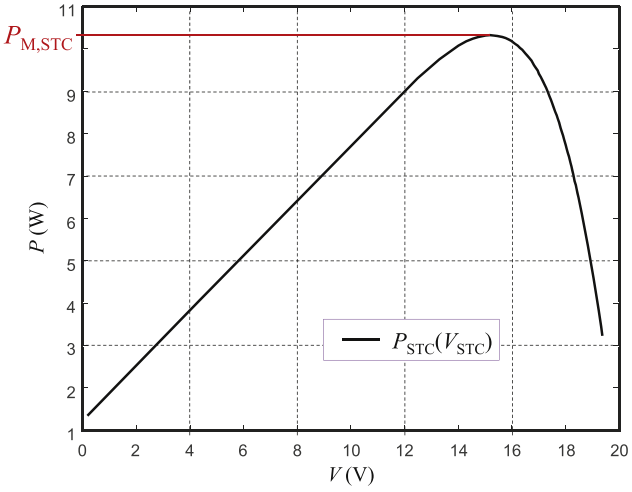

Fig. 3. Example of $P-V$ curve at STC.

Since the analytical description of the measurement model (2) is not trivial, the uncertainty of the parameter $P_{M,STC}$ due to the uncertainty of the measured quantities will be estimated through a numerical approach based on the Monte Carlo method [16], while the repeatability contribution will be estimated performing specific experimental tests.

3.1. Contribution of the measured quantities

The Monte Carlo method has been implemented by means of a MatLab script, in order to estimate the 95% confidence interval of the measured parameter $P_{M,STC}$. According to the specifications of the measurement equipment, which are summarized in the Section 2.3, for each Monte Carlo trial t the input quantities are obtained as:

$$I_{m,t} = I_{m0} \cdot (1 + \delta I_t) + I_{OFF,t}$$
$$V_{m,t} = V_{m0} \cdot (1 + \delta V_t) + V_{OFF,t}$$
$$G_{m,t} = G_{m0} \cdot (1 + \delta G_t) + G_{OFF,t} \quad (3)$$
$$T_{m,t} = T_{m0} + T_{OFF,t}$$

where

- I_{m0}, V_{m0} and G_{m0} are 100-size arrays acquired through the described experimental set-up in a time interval of about 10 s;
- T_{m0} is the cell temperature estimated from the measured environmental temperature;
- δI_t, δV_t and δG_t are realizations of normal probability distributions characterized by zero mean and standard deviation of $5 \cdot 10^{-4}$, $1 \cdot 10^{-5}$ and $6.5 \cdot 10^{-3}$, respectively;
- $I_{OFF,t}$, $V_{OFF,t}$, $G_{OFF,t}$ and $T_{OFF,t}$ are realizations of normal probability distributions characterized by zero mean and standard deviation of 20 μA, 5 μV, 3.5 W/m^2 and 1.0 °C, respectively.

Fig. 4 shows an example of distribution of $P_{M,STC}$ occurrences obtained using 5000 trials, which refers to a 10 W p-Si module characterized at an irradiance G_m of about 780 W/m^2. The results show the mean value and the standard deviation equal to 10.32 W and 0.08 W (about 0.8%) respectively, while the 95% confidence interval is (10.16–10.48) W.

The same procedure implemented on a 5 W p-Si module using the same measurement equipment has provided mean value and standard deviation equal to 5.40 W and 0.04 W (about 0.75%) respectively, while the 95% confidence interval is (5.32–5.47) W.

3.2. Repeatability contribution

The repeatability of the proposed test procedures has been estimated through repeated acquisition in similar conditions of $I-V$ curves of two different p-Si modules with nameplate power at STC equal to 5 W and 10 W. The $P-V$ curves at STC have been obtained implementing the procedure previously described to five $I-V$ curves acquired in outdoor conditions at an irradiance of about 950 W/m^2 and with air temperature of about 30 °C. For the 5 W module, the mean value of $P_{M,STC}$ is 5.40 W and the standard deviation is about 0.01 W, while for the 10 W module, mean and standard deviation values of $P_{M,STC}$ are 10.65 W and 0.025 W, respectively. Similar results have been obtained for other modules with the same nameplate specifications, thus showing that the repeatability contribution could be considered negligible with respect to the contributions related to the measured quantities.

3.3. Sensitivity coefficients

The results obtained in the Section 3.1 show that the 95% confidence interval of the parameter $P_{M,STC}$ could be of the same order of the degradation due to the applied stress factors. The obtained uncertainty is indeed ±1.6% and ±1.4% for the 10 W and 5 W modules, respectively. An analysis of each uncertainty contribution could be hence of interest in order to identify possible strategies that allow the overall uncertainty to be minimized. For this reason, the sensitivity coefficients c_x of the model (2) with respect to the measured quantities G_m, T_m, I_m and V_m have been estimated by approximating the partial derivatives with the ratio of the increments corresponding to small changes of each measured quantity. Such an estimation has been performed on experimental data obtained at different irradiance values for p-Si modules, obtaining the results that are summarized in the Fig. 5. The sensitivity coefficients reported in the figure are expressed in terms of percentage of the parameter $P_{M,STC}$ with respect to the absolute uncertainty for the measured quantities G_m and T_m and with respect to the relative uncertainty for the quantities I_m and V_m.

The results of the Fig. 5 show that the coefficients c_G (%/(W/m^2)) and c_T (%/(°C)) decrease as the irradiance increases, while the coefficients c_I and c_V (%/%) slightly increase as the irradiance increases. Assuming a negligible correlation coefficient

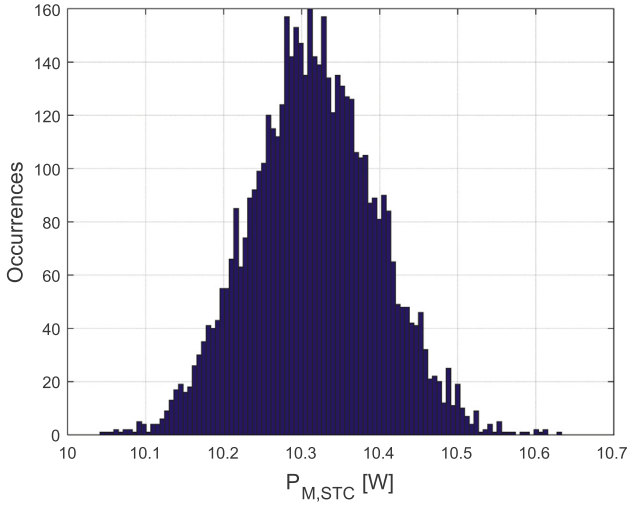

Fig. 4. Example of distribution of $P_{M,STC}$ occurrences of a 10 W p-Si module.

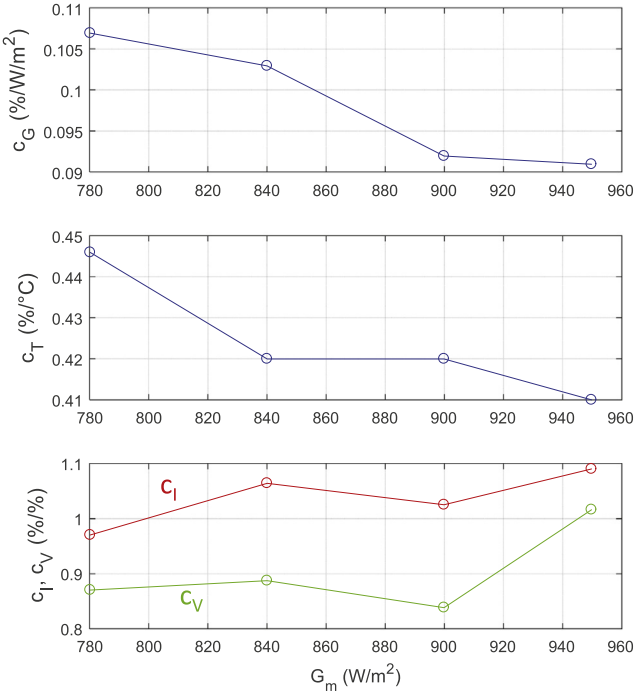

Fig. 5. Sensitivity coefficients of the model (2) with respect to the measured quantities for p-Si modules in the irradiance range (780–950) W/m^2.

between each couple of measured quantities, the relative percentage standard uncertainty $u_{r\%}(P_{M,STC})$ can be then estimated as:

$$u_r\%(P_{M,STC}) = \sqrt{c_G^2 \cdot u(G_m)^2 + c_T^2 \cdot u(T_m)^2 + c_I^2 \cdot \left[\frac{u(I_m)}{I_m}\right]^2 + c_V^2 \cdot \left[\frac{u(V_m)}{V_m}\right]^2} \quad (4)$$

If the expression (4) is implemented using the standard uncertainty of the measured quantities defined in the Section 2.3, the uncertainty contributions reported in the Table 1 are obtained, where $u_x(P)$ represents the relative uncertainty contribution of each measured quantity x to the estimated parameter $P_{M,STC}$. The obtained results show negligible differences in the overall uncertainty in the considered irradiance range, while interesting indications can be made comparing the different contributions: the

Table 1
Uncertainty contributions to the measured parameter $P_{M,STC}$ in the irradiance range (780–950) W/m^2.

G_m (W/m^2)	$u_G(P)$ (%)	$u_T(P)$ (%)	$u_I(P)$ (%)	$u_V(P)$ (%)	$u_{r\%}(P_{M,STC})$ (%)
780	0.917	0.446	0.049	$8.7 \cdot 10^{-4}$	1.02
840	0.923	0.420	0.053	$8.7 \cdot 10^{-4}$	1.01
900	0.860	0.420	0.051	$8.4 \cdot 10^{-4}$	0.96
950	0.880	0.410	0.054	$1.0 \cdot 10^{-3}$	0.97

Table 2
Nameplate specifications of the tested PV modules.

Type	m-modules	p-modules
Size	40 × 20 cm	30 × 25 cm
Cells in series	36	34
Strings in parallel	1	2
$P_{M,STC}$	10 W	5 W
$V_{M,STC}$	17.5 V	16.0 V
$I_{M,STC}$	0.58 A	0.30 A
$V_{oc,STC}$	22.2 V	20.2 V
$I_{sc,STC}$	0.64 A	0.33 A

uncertainty of the parameter $P_{M,STC}$ mainly depends on the measured quantities G_m and T_m, while the measurement uncertainties of the electrical quantities I_m and V_m give a negligible contribution.

The most effective intervention aimed at reducing the uncertainty of the parameter $P_{M,STC}$ seems to be a reduction of the irradiance measurement uncertainty $u(G_m)$, but this intervention has a very high cost, since a primary standard device should be used instead of the secondary standard pyranometer included in the measurement set-up arranged by the authors. Another effective intervention is the improvement in the measurement of the cell temperature T_m, which is now characterized by a standard uncertainty of 1 °C that is mainly due to the model used to estimate the cell temperature starting from the environmental temperature T_e

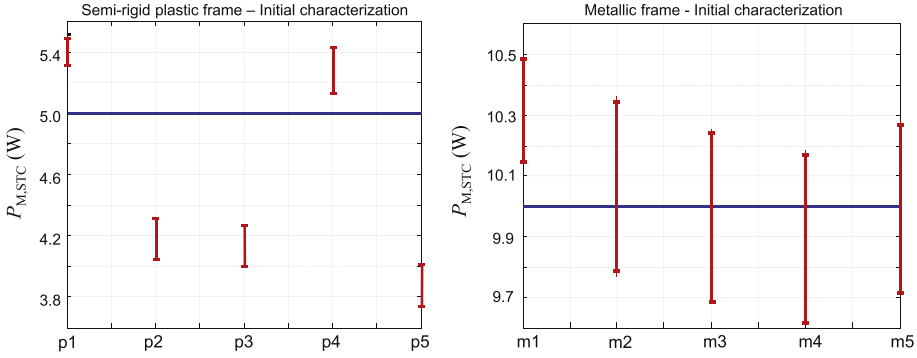

Fig. 6. Results of the initial electrical characterization of the tested PV modules: the vertical red bars are the 95% confidence interval of the parameter $P_{M,STC}$, while the horizontal blue lines are the nameplate maximum power at STC.

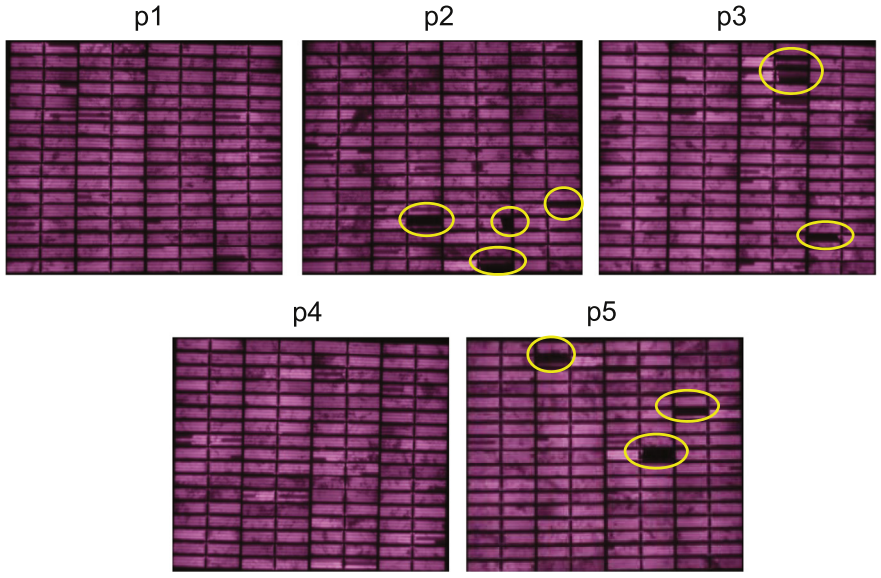

Fig. 7. Initial EL images of the modules p: the yellow circles in the p2, p3 and p5 images highlight the main defects. (For interpretation of the references to color in this figure legend, the reader is referred to the web version of this article.)

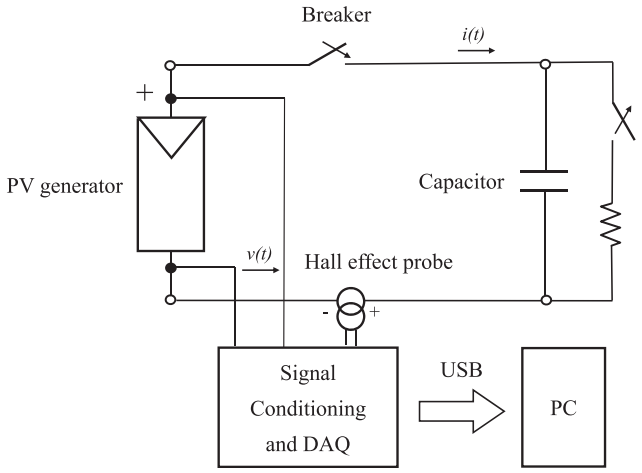

Fig. 8. Block scheme of the measurement set-up based on the capacitive-load technique.

and the module parameter *NOCT*. An alternative solution could be the measurement of the backside temperature of the PV module by means of a sensor thermally coupled to the backside surface of the module itself: in this case the parameter *NOCT* has not to be involved, but the measured temperature does not represent the actual cell temperature and the expected uncertainty is of the same order of the uncertainty obtained in the arranged set-up. These considerations highlight that the obtained uncertainty in the estimation of the parameter $P_{M,STC}$ can be hardly improved when a PV module is characterized in outdoor conditions.

4. Preliminary results

4.1. PV modules under test

The proposed test procedure has been implemented on two sets of p-Si modules: the first set includes five front-glass modules with a metallic frame, hereafter referred as m-modules, while the second set includes five semi-rigid plastic modules, hereafter referred as p-modules. The Table 2 reports the nameplate specifications of the tested PV modules. The choice of low-size and low-power PV modules is related to the dimensions of climatic chamber and electrodynamic shaker that have been used to generate the stress quantities.

4.2. Initial characterization

Before applying environmental and mechanical stresses to the investigated PV modules, their $I-V$ characteristics and their EL images have been obtained. The results that refer to the initial electrical characterization of each module are reported in Fig. 6, where the vertical red bars are the 95% confidence intervals of

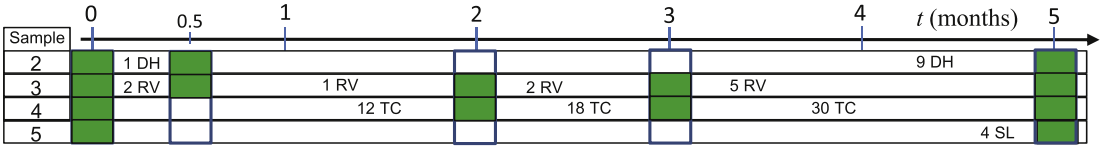

Fig. 9. Summary of the tests carried out on the investigated PV modules over a five-month period.

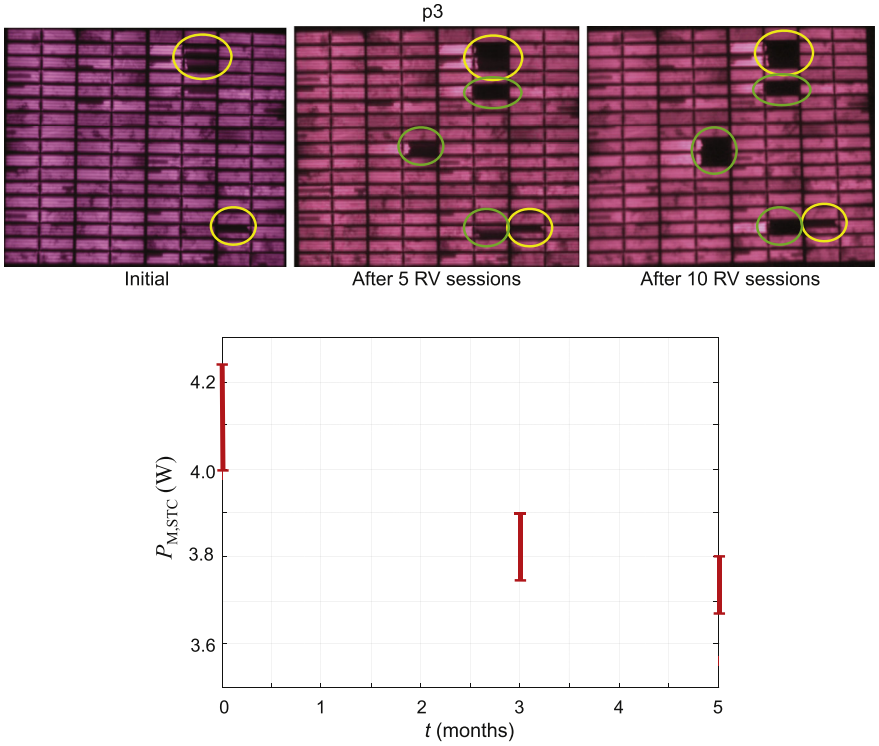

Fig. 10. Evolution of the defects in the PV module p3 due to the dynamic mechanical stress and corresponding results of the electrical characterization.

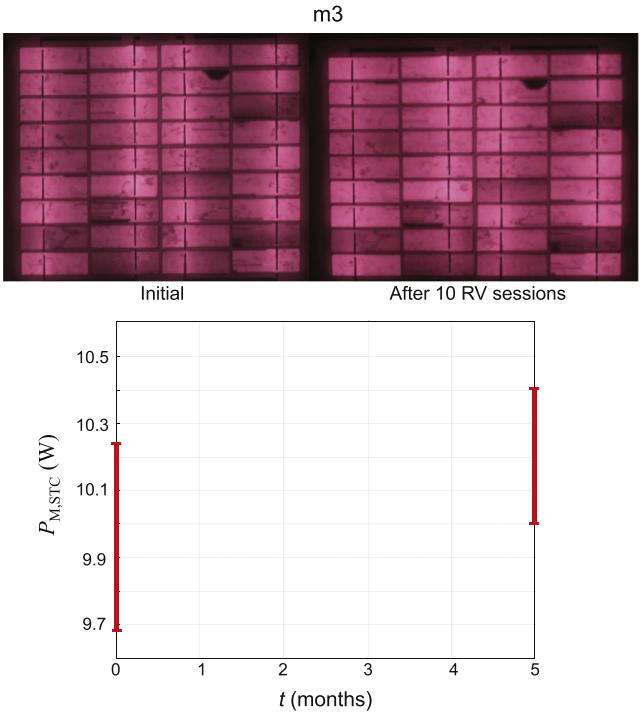

Fig. 11. EL images and corresponding results of the electrical characterization of the PV module m3 before and at the end of the dynamic mechanical stress.

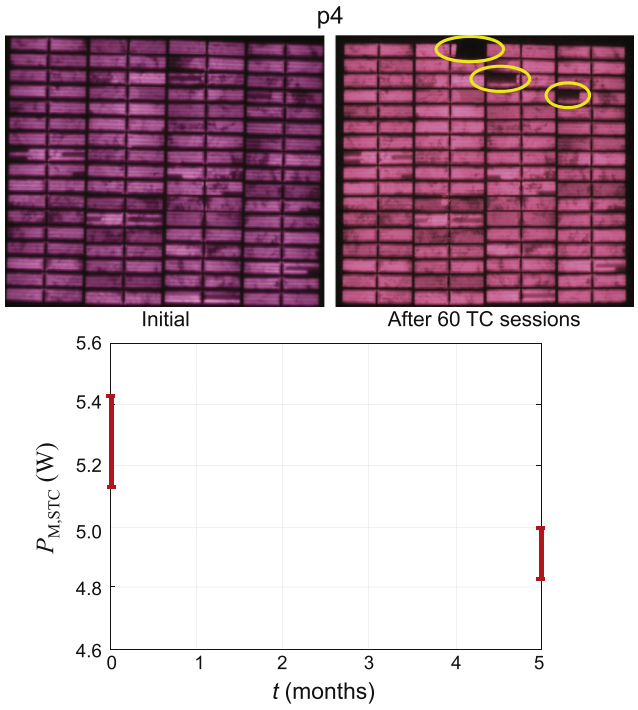

Fig. 13. EL images and corresponding results of the electrical characterization of the PV module p4 before and at the end of the thermal stress.

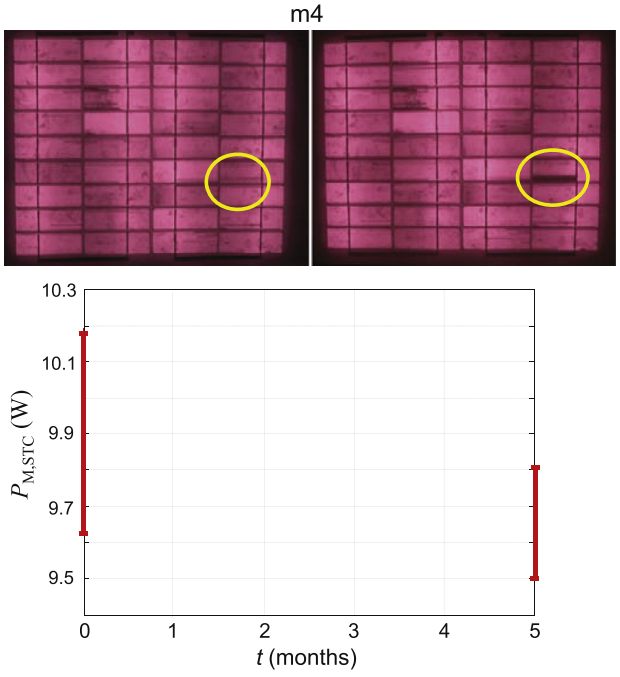

Fig. 12. Evolution of the defects in the PV module m4 due to the thermal stress and corresponding results of the electrical characterization.

the parameter $P_{M,STC}$, while the horizontal blue lines are the nameplate maximum power at STC. One should note that m-modules (right-side of the figure) are conform to their nameplate specification. On the contrary, three of the p-modules (p2, p3 and p5) show lower performance than the nameplate specifications (left-side of the figure). This result is in agreement with the obtained EL images: Fig. 7 shows the images obtained for the p modules, where the presence of important defects in the modules p2, p3 and p5 is highlighted.

From the results reported in the Fig. 6, one should note that the confidence intervals of the parameter $P_{M,STC}$ of the modules p1 and m1 are lower than the confidence interval of the other modules. This is due to a different measurement set-up that was initially used to characterize the PV module, which is based on the capacitive-load technique [17,18] and whose block scheme is shown in Fig. 8. It is based on a Data Acquisition (DAQ) system that simultaneously detects the voltage across the PV module under test and the current the module provides during the transient charge of an electrolytic capacitor, thus obtaining the $I - V$ characteristic of the module in a time interval that does not exceed 100 ms. During this interval, the DAQ system also acquires irradiance and temperature values. However, this setup was tailored for PV modules that exhibit larger power, and the current measurements, which are obtained through a Hall effect current probe, are affected by a relative uncertainty larger than 1% [19]. The initial characterization of the modules p1 and m1 has been repeated using the set-up based on the programmable electronic load, but the same was not possible for the other modules that have been subjected to stress tests.

4.3. Preliminary stress results

The two sets of investigated PV modules have been subjected to a first series of stress tests over a period of five months, as specified below:

- modules p2 and m2: ten cycles of damp-heat (DH) test – total test time: 240 h;
- modules p3 and m3: ten random-vibration (RV) sessions – total test time: 50 h;
- modules p4 and m4: sixty thermal cycles (TC) – total test time: 240 h;
- modules p5 and m5: 4 days of static load (SL).

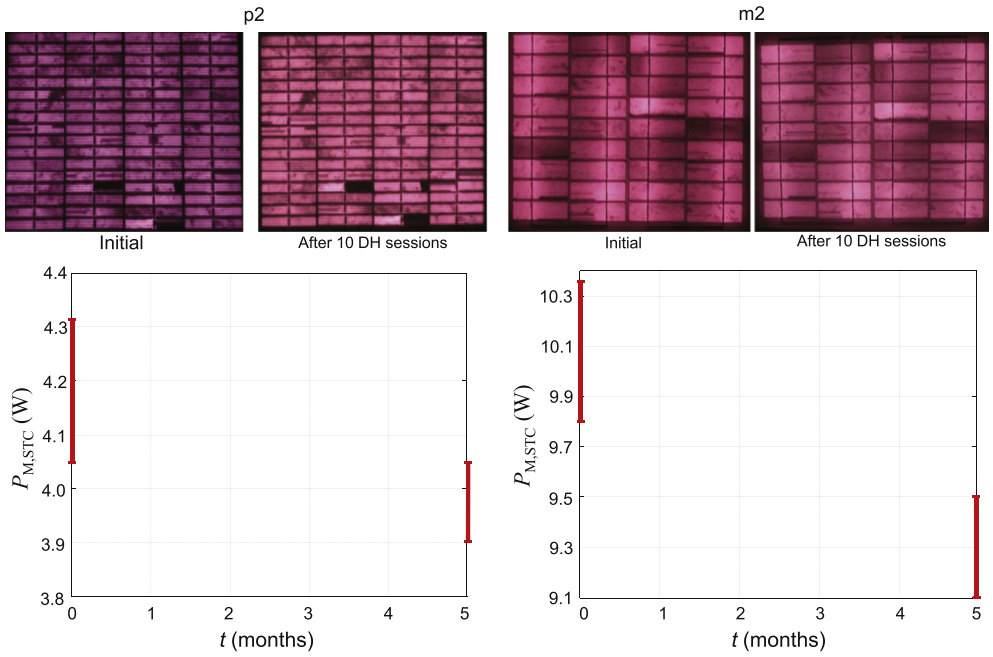

Fig. 14. EL images and corresponding results of the electrical characterization of the PV modules p2 and m2 before and at the end of the damp heat stress.

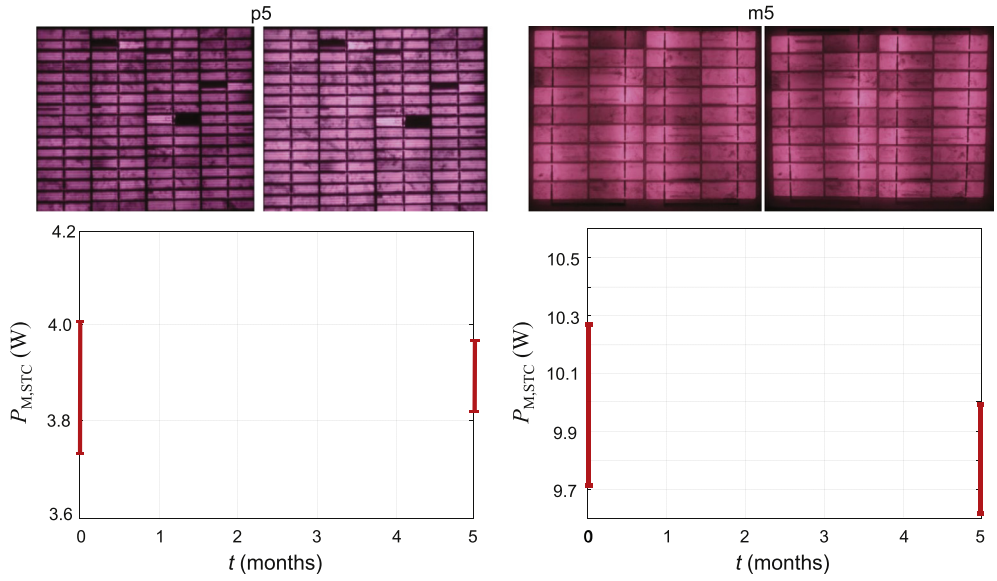

Fig. 15. EL images and corresponding results of the electrical characterization of the PV modules p5 and m5 before and at the end of the static load stress.

A summary of the performed tests is shown in the Fig. 9, where the dark boxes tag the instants the characterization of the PV modules has been performed.

The Fig. 10 summarizes the results obtained for the PV module p3, which was subjected to dynamic mechanical stress. The EL images in the upper part of the figure highlight the evolution of the initial defects present in the PV module (yellow[1] circles) and show other broken cells (green circles) that arose after two series of five random-vibration sessions. The electrical characterization (bottom part of the figure) provided results that are in agreement with the EL images: the relative change of the parameter $P_{M,STC}$ with respect to the initial value was of −9.7%.

The front-glass module m3, which was subjected to the same dynamic mechanical stress, did not show significant $P_{M,STC}$ degradation and its EL image at the end of the stress cycle was almost the same as the initial EL image, as shown in Fig. 11.

The results in the Fig. 12 show the evolution of EL and electrical characterizations of the PV module m4, which was subjected to sixty thermal cycles. In this case, the EL image highlights a defect that arose at the end of the stress test and the parameter $P_{M,STC}$ had a decrease of −2.5%. However, this result is made questionable by the measurement uncertainty, that was larger for the initial

[1] For interpretation of color in Fig. 10, the reader is referred to the web version of this article.

characterization due to the different experimental set-up. The same thermal stress applied to the semi-rigid plastic module p4 resulted in a relative change of the parameter $P_{M,STC}$ of −6.5%. The EL images and the results of the electrical characterization of the module p4 are shown in the Fig. 13, where the yellow circles highlight the defects that arose after sixty thermal cycles.

Both the PV module p2 and m2 exhibited a significant degradation consequent to the damp-heat test (240 h), with a relative change of the parameter $P_{M,STC}$ of −5.0% and −7.8%, respectively. In this case, the EL images, which are shown in the upper part of the Fig. 14, do not allow this degradation to be observed, since the effect of this stress consists in decreasing the electrical insulation of the module without causing damages of the cells.

Eventually, for the module p5 and m5 that were subjected to a continuous static load for a four-day interval, no significant degradation was observed, since the relative change of $P_{M,STC}$ was of the same order of the measurement uncertainty. Also the EL images, which are shown in the upper part of the Fig. 15, do not show significant damages to the cells of the two PV modules.

5. Conclusion

A test procedure has been proposed in this paper that is conceived to estimate the degradation rate of PV modules subjected to mechanical and environmental stresses. Particular attention has been paid towards uncertainty issues in order to correctly interpret the obtained results, which are expressed in terms of maximum power of the PV module at Standard Test Conditions ($P_{M,STC}$). Useful suggestions have been provided that allow the metrological specifications of the employed equipment to be selected.

The proposed measurement set-up, which is based on a programmable electronic load, allows the parameter $P_{M,STC}$ to be obtained with a relative standard uncertainty of about 1%. One should note that such an uncertainty value represents a lower limit when the characterization of PV modules in outdoor conditions is performed, since it is mainly due to the uncertainty contributions of irradiance and cell-temperature measurements, which can be improved only in laboratory conditions. Preliminary tests, which have been performed on two sets of p-Si modules, have shown the effectiveness of the proposed procedure: the degradation of the parameter $P_{M,STC}$ was higher than the corresponding uncertainty for almost all the applied stresses and the EL images have confirmed the obtained results. Between the two kinds of tested modules, the ones encapsulated in a semi-rigid plastic frame (p-type) have shown a higher sensitivity to dynamic mechanical stresses, with a relative change of $P_{M,STC}$ of about −9.7% after 50 h of random vibration stress. The same stress applied to a front-glass module with a metallic frame (m-type) did not produce a significant degradation, thus highlighting that the effects of dynamic mechanical stresses on the same PV technologies strongly depend on the module frame. The p-type module also exhibited a higher sensitivity with respect to the thermal stress than the m-type module: after sixty thermal cycles in the range of −20 °C to 70 °C (temperature rate of about 1 °C/ min) the relative change of $P_{M,STC}$ was of about −6.5% for the former and of −2.5% for the latter.

With respect to the damp-heat stress, after 240 h of exposure of the PV modules to environment at high temperature and high relative humidity, a significant degradation has been observed. In this case the m-type module have shown the higher sensitivity, with a relative change of $P_{M,STC}$ of about −7.8%, while the relative change of the same parameter for the p-type module was of about −5.0%. This result provides information about the sealing strength of the two modules, which seems to be better for the p-type module that is covered with an insulating coating.

Eventually, static loads had no important effects on both types of modules.

The proposed procedure will enable the authors to estimate the degradation rate of commercial PV modules characterized by larger power than the two set of modules here investigated, thanks to set facilities that allow the stress quantities to be applied to modules of larger size. This will allow thin-film based modules to be also tested, thus having the possibility of confirming the results obtained in the outdoor experimental PV laboratory.

References

[1] International Energy Agency, Photovoltaic Power Systems Technology Collaboration Programme – Annual report, 2015.

[2] E.D. Dunlop, D. Halton, The performance of crystalline silicon photovoltaic solar modules after 22 years of continuous outdoor exposure, Prog. Photovolt.: Res. Appl. 14 (2006) 53–64.

[3] A. Skoczek, T. Sample, E.D. Dunlop, The results of performance measurements of field-aged crystalline silicon photovoltaic modules, Prog. Photovolt.: Res. Appl. 17 (2009) 227–240.

[4] D.C. Jordan, S.R. Kurtz, Photovoltaic degradation rates – an analytical review, Prog. Photovolt.: Res. Appl. 21 (2013) 12–29.

[5] E. Lorenzo et al., Performance analysis of a 7-kW crystalline silicon generator after 17 years of operation in Madrid, Prog. Photovolt.: Res. Appl. (2013), http://dx.doi.org/10.1002/pip.2379.

[6] A. Carullo, S. Corbellini, A. Luoni, A. Neri, In situ calibration of heterogeneous acquisition systems: the monitoring system of a photovoltaic plant, IEEE Trans. Instrum. Meas. 59 (5) (2010) 1098–1103.

[7] A. Carullo, A. Vallan, Outdoor experimental laboratory for long-term estimation of photovoltaic-plant performance, IEEE Trans. Instrum. Meas. 61 (5) (2012) 1307–1314.

[8] A. Carullo et al., Uncertainty analysis of degradation parameters estimated in long-term monitoring of photovoltaic plants, Measurement 55 (2014) 641–649, http://dx.doi.org/10.1016/j.measurement.2014.06.003.

[9] M. Paggi, M. Corrado, M.A. Rodriguez, A multi-physics and multi-scale numerical approach to microcracking and power-loss in photovoltaic modules, Compos. Struct. 95 (2013) 630–638.

[10] G. Makrides et al., Temperature and thermal annealing effects on different photovoltaic technologies, Renewable Energy 43 (2012) 407–417.

[11] J. Schlothauer, S. Jungwirth, M. Kohl, B. Roder, Degradation of the encapsulant polymer in outdoor weathered photovoltaic modules: spatially resolved inspection of EVA ageing by fluorescence and correlation to electroluminescence, Sol. Energy Mater. Sol. Cells 102 (2013) 75–85.

[12] International Standard IEC 61215:2005-04, Crystalline silicon terrestrial photovoltaic (PV) modules – Design qualification and type approval, second ed. (2005-04).

[13] A. Carullo, A. Vallan, A. Ciocia, F. Spertino, Degradation test and characterization procedures of photovoltaic modules exposed to outdoor conditions, in: Proceedings of XXXI IMEKO World Congress, August 30 – September 4, 2015, Prague, Czech Republic, 2015.

[14] Standard IEC 60904-9:2007-10, Photovoltaic devices – Part 9: Solar simulator performance requirements.

[15] Standard IEC 60891:2009-12, Photovoltaic devices – Procedures for temperature and irradiance corrections to measured I-V characteristics.

[16] 101:2008, JCGM. Evaluation of measurement data – Supplement 1 to the Guide to the expression of uncertainty in measurement – Propagation of distributions using the Monte Carlo method.

[17] F. Attivissimo et al., On the performance of the double-diode model estimating the maximum power point for different photovoltaic technologies, Measurement 46 (3) (2013) 3549–3559.

[18] F. Spertino, J. Sumaili, H. Andrei, G. Chicco, PV module parameter characterization from the transient charge of an external capacitor, IEEE J. Photovolt. 3 (2013) 1325–1333.

[19] A. Carullo, A. Castellana, A. Vallan, A. Ciocia, F. Spertino, Experimental assessment of degradation rate in photovoltaic modules, in: Proceedings of 21st IMEKO TC4 Internatinal Symposium, September 7–9, Budapest, Hungary, 2016.